Respiratory Physiology & Neurobiology 262 (2019) 40–48

Contents lists available at ScienceDirect

Respiratory Physiology & Neurobiology

journal homepage: www.elsevier.com/locate/resphysiol

Experimental and numerical investigation on inspiration and expiration flows in a three-generation human lung airway model at two flow rates

Zhenshan Zhu[a], Chuhua Zhang[a,b,*], Li Zhang[c]

[a] Department of Fluid Machinery and Engineering, School of Energy and Power Engineering, Xi'an Jiaotong University, Xi'an, Shaanxi, People's Republic of China
[b] State Key Laboratory for Strength and Vibration of Mechanical Structures, Xi'an Jiaotong University, Xi'an, Shaanxi, People's Republic of China
[c] China Academy of Space Technology, Xi'an, Shaanxi, People's Republic of China

ARTICLE INFO

Keywords:
Tracheobronchial model
Three-generation airway model
Inspiration flow
Expiration flow
LDV measurements
CFD simulations

ABSTRACT

The respiration flow pattern plays a key role in fluid flow, heat and mass transfer in human lung airway. To reveal the complex flow pattern within human lung multiple-generation airway, both the steady inspiration and expiration flows are comprehensively studied using laser Doppler velocimetry technique and computational fluid dynamics method for an idealized human tracheobronchial three-generation airway model at two flow rates, corresponding to an adult male breathing under light activity and moderate exercise conditions, respectively. The comparison of mainstream velocity between the measurements and simulations are generally good. Both of the inspiration and expiration flows are heavily influenced by the combination of geometrical bifurcating/merging, local wall curvature, limited generation length and multi-generation interaction. The mainstream flow is non-uniform and behaves as skewed, double-peaked and M-shaped patterns. The secondary flow is complex and characteristic of Dean-type two-vortex, four-vortex, six-vortex and eight-vortex patterns. This work is of scientific significance for a deep understanding of respiratory flow physics and of certain application values for clinical diagnosis and remedy of respiratory deceases.

1. Introduction

The respiration flow in human lung airway is one of the most basic and revealing problems in the fields of biological fluid mechanics and biological mechanical engineering. The human lung airway is virtually an upside-down tree of multiple generations of branching tubes. According to the directions of breathing flows, the respiration flow can be decomposed into two successive and alternate flow stages, i.e., inspiration flows and expiration flows, both of which are closely related with the respiration anatomy, breathing flow rate, environmental condition, etc. A detailed analysis of the inspiration and expiration flow fields in human lung airway is among the hot topics in the experimental fluid dynamics (EFD) and computational fluid dynamics (CFD). The related research works are of scientific significance for a deep understanding of respiration physics, physiology and pathology, and of clinical application values for control optimization of aerosol drug transportation and design optimization of artificial breathing machine.

Several experimental works have been performed for the flow velocity in branching tubes by using measurement techniques, such as LDV (laser Doppler velocimetry, also known as LDA, i.e., laser Doppler anemometer), PIV (particle image velocimetry) and MRI (magnetic resonance imaging). Große et al. (2007) constructed a transparent silicone TB (tracheobronchial) airway model and applied PIV technique to measure the steady and unsteady mainstream velocity in the G_0 and G_1 region at Reynolds number (*Re*) of 1050, 1400 and 2100. They pointed out that the overall flow patterns were nearly independent of the *Re* under consideration, and the unsteady flow velocity profile at each measured constant was quite similar to the steady one at equivalent *Re*. The similar PIV work was also performed at *Re* of 673–4039 by Adler and Brücker (2007), who found that the inspiration flows in the trachea were not much influenced by the asymmetry of the daughter branches and behaved as nearly symmetric flow patterns. Recently, Banko et al. (2015) constructed a computed tomography (CT) scanned model for the upper and TB airways, and applied MRI technique to measure the inspiration flow velocity in G_0 and G_1 at $Re = 4200$. They stated that, at low and moderate oscillation frequencies, the effect of unsteadiness should be minor in the human lung airway. Most of the above planar measurements (PIV and MRI), however, were focused on the mainstream velocity at the region of G_0 and G_1.

* Corresponding author at: Department of Fluid Machinery and Engineering, School of Energy and Power Engineering, Xi'an Jiaotong University, No. 28 West Xianning Road, Xi'an, 710049, Shaanxi, People's Republic of China.
E-mail address: chzhang@mail.xjtu.edu.cn (C. Zhang).

https://doi.org/10.1016/j.resp.2019.01.012
Received 21 October 2018; Received in revised form 10 January 2019; Accepted 26 January 2019
Available online 30 January 2019

LDV is an even more suitable candidate to accurately measure the flow fields with high resolution and capable of providing reliable validation data for detailed CFD simulations (Lizal et al., 2018). Zhao and Lieber (1994a, 1994b) were among the first one who applied LDV technique to measure the inspiration and expiration flows in a 70° two-generation symmetric airway model with water as the working fluid. They reported that the inspiration and expiration mainstream velocity profiles in the daughter branches were skewed towards the inner wall. Later, Farag et al. (2000) used LDV technique to measure the inspiration flows in a two-generation symmetric airway model with air as the working fluid. They found that the detailed geometry of transition between the parent and daughter branches as well as bifurcating angle and wall curvature played important roles in bifurcating flow. Recently, Kerekes et al. (2016) have performed LDV measurements and CFD simulations of the inspiration flow characteristics of G_0-G_2 in an idealized TB model with mixture of water and glycerol as the working fluid. However, their multi-generation model adopted straight circular tubes in each generation and sharp transition between successive generations, which are non-physiological anatomic. In summary, most of the LDV measurements were performed for the inspiration flows. The LDV measurements of the respiration flows at various flow rates were less mentioned.

From the above reviews, quite few works are denoted to the simultaneous measurements and simulations of the inspiration and expiration flows in three-generation TB model (G_0-G_2) at various flow rates. The CFD method validated with the reliable measurements can provide much more flow details which could be hardly, if not impossible, captured by measurement techniques (Jalal et al., 2016). A comprehensive experimental and numerical analysis of the inspiration and expiration flows at real physiological breathing rates will be very helpful for a deep understanding of the physiology and pathology of respiration system and the associated flow interaction between the successive generations in human lung airway.

The *Re* in TB model varies greatly depending on the breathing rate and local geometry size, and thus a choice of viscous flow model is crucial to the CFD method. Liu et al. (2002, 2003) adopted the three dimensional incompressible Navier-Stokes equations with laminar flow model to calculate the respiratory flows in symmetric and asymmetric three-generation airway models (G_5-G_7) at the *Re* range of 200-1600. Li et al. (2017) observed that the laminar model predictions matched well with the experimental data at rest breathing rate. Jalal et al. (2016) reported that the flows in their TB model (G_0-G_2) presented turbulent ones with $Re \geq 3000$. Zhang and Kleinstreuer (2003) suggested that the k-ω model (Menter, 1994) with low-Reynolds-number (LRN) effect corrections was more suitable for the respiration flow in human airway TB model, while Jayaraju et al. (2007) found LRN SST (Shear Stress Transport) k-ω model may perform better in the numerical simulation of transitional flows. In order to find out the appropriate viscous model for the TB airway, totally six viscous models are compared in the present CFD simulations.

In this study, both of the LDV technique and CFD method are used to investigate the inspiration and expiration flows in a three-generation TB model (G_0-G_2) at two typical flow rates of 30 L/min and 60 L/min, corresponding to an adult male breathing under light activity and moderate exercise conditions, respectively (Adams et al., 2018). The TB measurement rig is composed of inlet, inspiration, expiration and outlet segments. Totally fifteen cross sections are measured using LDV and a detailed comparative analysis between the LDV measurements and CFD simulations is performed.

This paper is organized as follows. In Section 2, the geometry of a TB model will be briefly introduced. Sections 3 and 4 will outline the experimental technique and CFD method, respectively. The results of the measurements and simulations will be depicted and discussed in Section 5. Some concluding remarks will be drawn in Section 6.

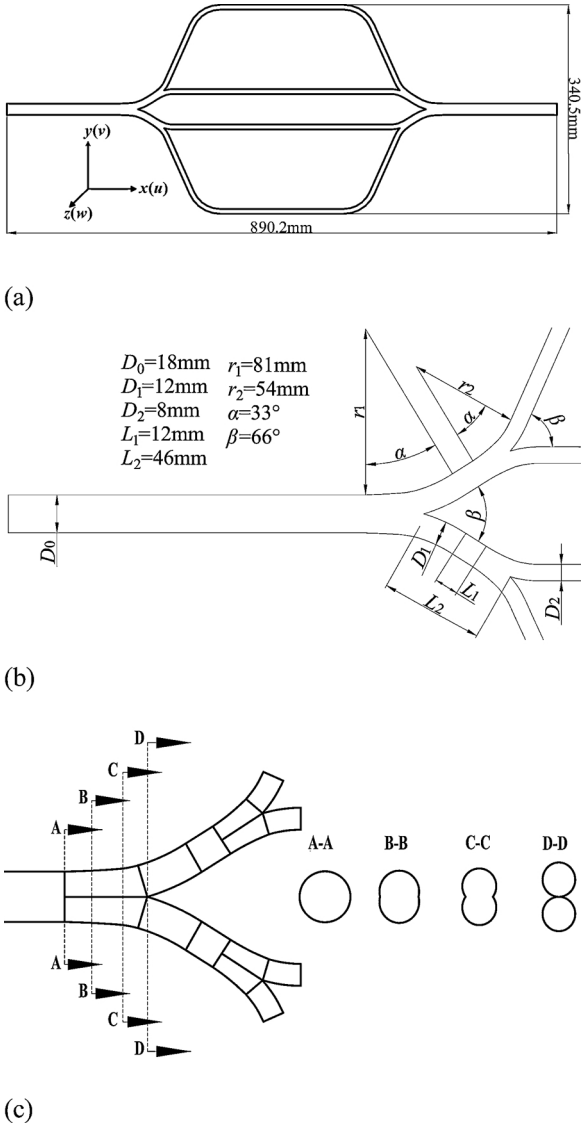

Fig. 1. The three-generation TB airway model: **(a)** global view; **(b)** main parameters; **(c)** typical cross sections at the transition zone.

2. Geometry model

The respiration tract of human lung is essentially a network of repeatedly bifurcating airways. An idealized TB model is taken in this work. Several researchers confirmed that the idealized model is a suitable one to capture the essential flow properties at the G_0-G_3 of TB model (Kleinstreuer and Zhang, 2009, 2010). The idealized three-generation TB airway model under consideration is constructed with the measured or compiled data of human lung airway anatomy in Weibel (1963); Pedley (1977); Kleinstreuer et al. (2008); Jalal et al. (2016); Kerekes et al. (2016); Schiavazzi et al. (2017).

Figure 1 presents the idealized human lung three-generation TB airway model. The geometry model can provide the same mass flow rates at the expiration flow inlets and the inspiration flow outlets. In order to avoid or weaken the mutual influences of the inspiration and expiration segments, the experimental rig is designed large enough, i.e., 890.2 mm long and 340.5 mm width (Fig. 1a). As for the geometry details in Fig. 1(b), the curvature radii are $r_1/(D_0/2) = 9$ and $r_2/(D_1/2) = 9$, or $r_1/D_1 = 6.75$ and $r_2/D_2 = 6.75$, respectively, and the bifurcating angle of both the G_0-G_1 and G_1-G_2 transition is 66°. The diameters of G_0, G_1 and G_2 tubes are 18 mm, 12 mm and 8 mm, respectively. The length-to-diameter ratio L_1/D_1 at the G1 is about 3.8.

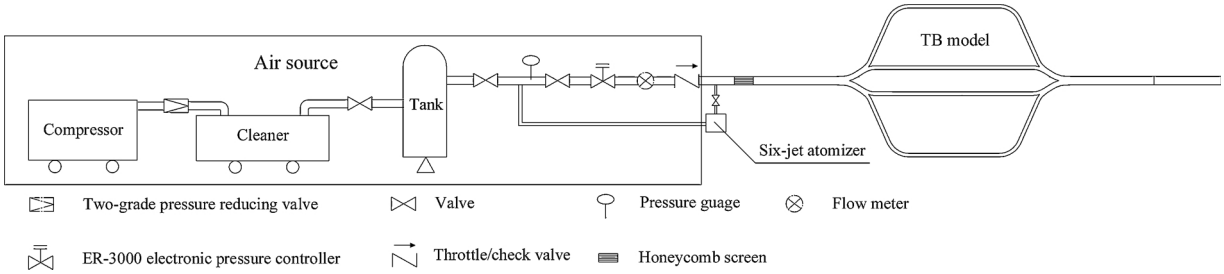

Fig. 2. Schematic of experimental setup. The whole experimental system is composed of air source, aerosol trace particle filling system and the measurement segment.

Fig. 1(c) shows the typical evolution of cross sections at the transition zone, which vary from circular (cross section A-A), elliptical (cross section B-B), eight-shaped (cross section C-C) and finally the mother branch is divided into two daughter circular ones (cross section D-D). The cartilage rings, C-shaped rings and the other affiliated substances in realistic trachea are all ignored in the current idealized model.

3. Experimental technique

The objectives of the present experimental study are to measure the flow velocity profiles at the representative cross sections within the inspiration and expiration segments using LDV technique, and to provide the validation data for the CFD simulation. The working fluid is the air. Fig. 2 presents the schematic of experimental setup. The photo of the measurement segment together with two LDV probes is shown in Fig. 3.

The air source system plays an important role in supplying highly stable and accurately controllable air conditions for the measurement segment. To this point, a two-grade pressure-reducing valve, a manually controllable throttle/check valve and an electronic pressure controller ER-3000 are used. A honeycomb screen is inserted upstream the measurement segment to ensure a more uniform air flow. The fluctuations in flow rates monitored by an orifice flow meter are estimated within ± 0.5%.

A six-jet atomizer (model 9306, TSI) is used to generate the tracer droplets with mean diameter of 0.3 μm, standard deviation of less than 2.0 and particles concentration of over $10^8/cm^3$. The atomizer can offer an adjustable flow rate from 1.0 to 4.2 L/min. The tracer particle is chosen as Glycerin and has the advantages of good fluid following and laser scattering.

The measurement segment is machined from a whole brick of PMMA (Polymethyl Methacrylate) by using the computerized numerical control (CNC) machining technique. The refractive index of PMMA is 1.49. The wall thickness of airway model is 0.8 mm. The manufacture tolerance of the measurement segment is estimated within ± 0.1%. To avoid environmental impact, two circular tubes with sufficient length

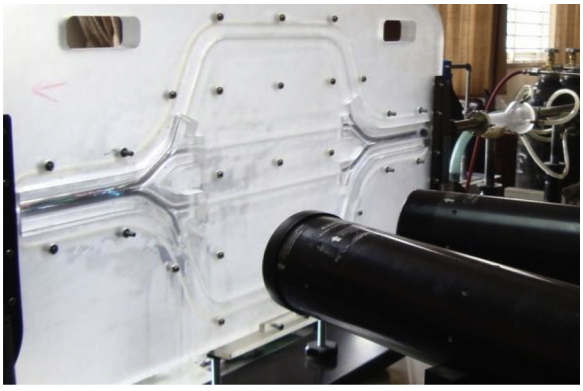

Fig. 3. Photo of the measurement segment and two 3D LDV probes.

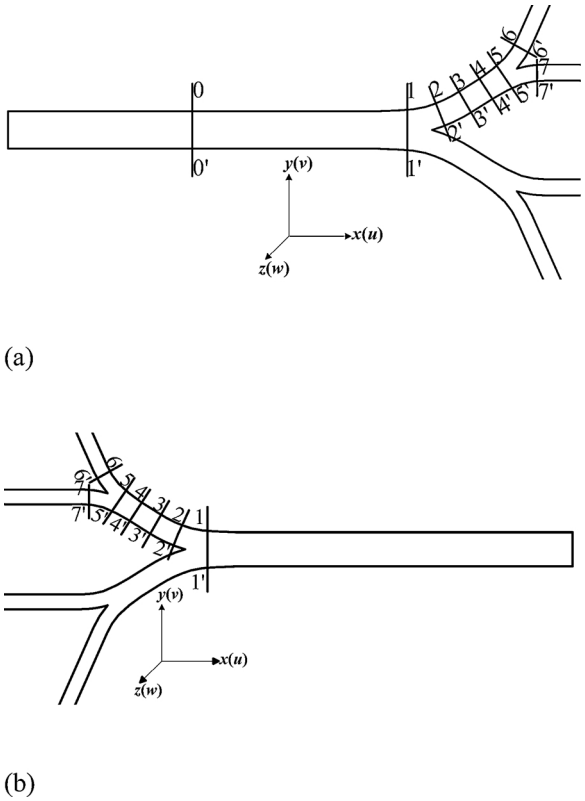

Fig. 4. The measurement cross section positions: **(a)** eight cross sections in the inlet and inspiration segments; **(b)** seven cross sections in the expiration segment.

are attached before and after the measurement segment, respectively.

The LDV technique (model 9253-350, TSI) is adopted to measure the inspiration and expiration mainstream velocity in the measurement segment (Fig. 3). Based on the expected variation in flow velocity, totally fifteen cross sections are measured, the positions of which are shown in Fig. 4 and listed in Table 1. At each measurement point, three

Table 1
Length-to-diameter ratios (L/D) of the cross sections at the inlet (cross section 0′-0), inspiration and expiration segments (cross section 1'-1 to 7′-7). L_1 and L_2 are refer to the axial tube lengths of one cross section to the first bifurcation (G_0-G_1) and the second bifurcation (G_1-G_2), respectively. And D is the local generation diameter of the cross section. The position L/D = 0.0 is assumed at the bifurcation, with minus and positive signs indicating locations upstream and downstream, respectively.

	Cross section 0'-0	1'-1	2'-2	3'-3	4'-4	5'-5	6'-6	7'-7
L_1/D	−7.0	−0.6	0.5	1.5	2.4	3.2		
L_2/D			−3.3	−2.3	−1.4	−0.6	1	1

perpendicular flow velocity components are measured from a series of 1000 valid signals recorded by LDV counter processors. A good repeatability of the experimental results is confirmed, and the variability coefficient is estimated within 1%. According to the methods in Durst et al. (1981); Corcoran and Chigier (2002); Zhang (2010); Lizal et al. (2018), the shift in measured probe positioning is calculated to be within 0.2 mm, which is negligible small relative to the model dimension.

4. Numerical model

Respiration flow in human lung airway is very complicated due to complex geometry and anatomy in human airway. Moreover, the flow in human lung airway may undergo different flow regimes, i.e., laminar, transitional and turbulent flows, in different airway generations.

The CFD method validated with the reliable measurements can provide much more flow details than the pure measurement techniques. In order to find out the most appropriate viscous model for the numerical simulation of respiration flows at TB model, totally six viscous models including the laminar, S-A (Spalart-Allmaras), k-ε, RNG k-ε, LRN k-ω and LRN SST k-ω models are tested. The comparison of the numerical predictions with the experimental data shows that the LRN SST k-ω model performs generally better at the flow rate of 60 L/min than other viscous models while the laminar model fits better the measurements at 30 L/min. At the flow rates 30 L/min and 60 L/min, the Re numbers are 2205 and 4410, respectively. It can be inferred that the viscous flow is even closer to the laminar one at the flow rate of 30 L/min (light activity condition) while the turbulent one at 60 L/min (moderate exercise condition). For the sake of comparison between the numerical and experimental results, the inlet boundary mainstream velocity components at the inlet of TB model (cross section 0′-0) are interpolated from the experimental results. The static pressure and non-slip boundary conditions are specified at the outlet and the wall, respectively.

High-quality block-structured grids are generated with commercial software Gambit. Firstly, the whole TB flow domain is divided into 65 relatively simple sub-domains. Secondly, each sub-domain is further discretized into structured grid elements with fine mesh in the solid wall boundary layer. Finally, all the sub-domain meshes are merged into the whole gird. To obtain grid-independence results, three types of grids are employed, i.e., coarse, midst and fine grid with mesh element number 3.39 million, 6.75 million and 10.57 million, respectively. From the inspiration mainstream velocity profiles along the 3′-3 line, the grid-independence results can be obtained with midst grid, and thus the midst grid is adopted in the following simulations (Fig. 5). About 98.5% of wall y^+ values of the first layer meshes adjacent to solid walls are less than 1.

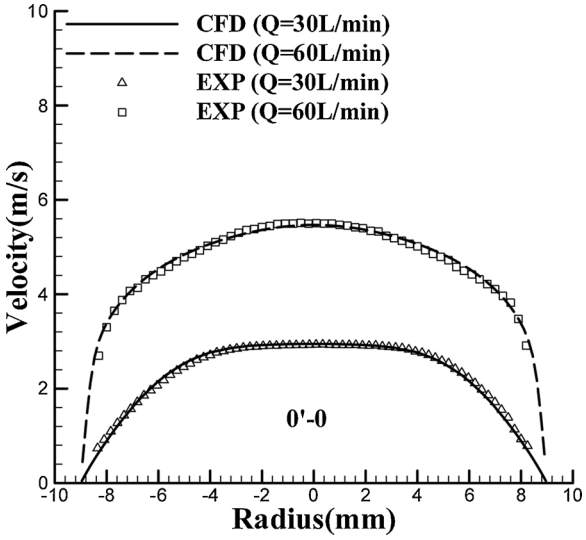

Fig. 6. The inspiration mainstream velocity profiles at the inlet cross section 0′-0.

The commercial CFD software ANSYS-Fluent 15.0 is applied to numerically solve the governing equations using finite volume method. The convective term is discretized by QUICK scheme while the diffusive and pressure terms by the second-order central scheme. The velocity and pressure coupling are treated through the SIMPLE algorithm. All of the numerical cases are performed on an Inspur server with twelve-core Intel CPUs (central processing unit), and the averaged CPU times are about 6 h and 15 h at the laminar and LRN SST k-ω models, respectively.

5. Results and discussion

The experimental and numerical results of the inspiration and expiration flows in the three-generation TB model at the two typical flow rates of 30 L/min and 60 L/min are presented in Figs. 6–9 and discussed in this section. Together with the comparisons of the mainstream velocity between the experimental and numerical results, the numerical simulations of secondary flow vortex are also presented.

5.1. Inspiration

The inlet boundary condition for the mainstream velocity is

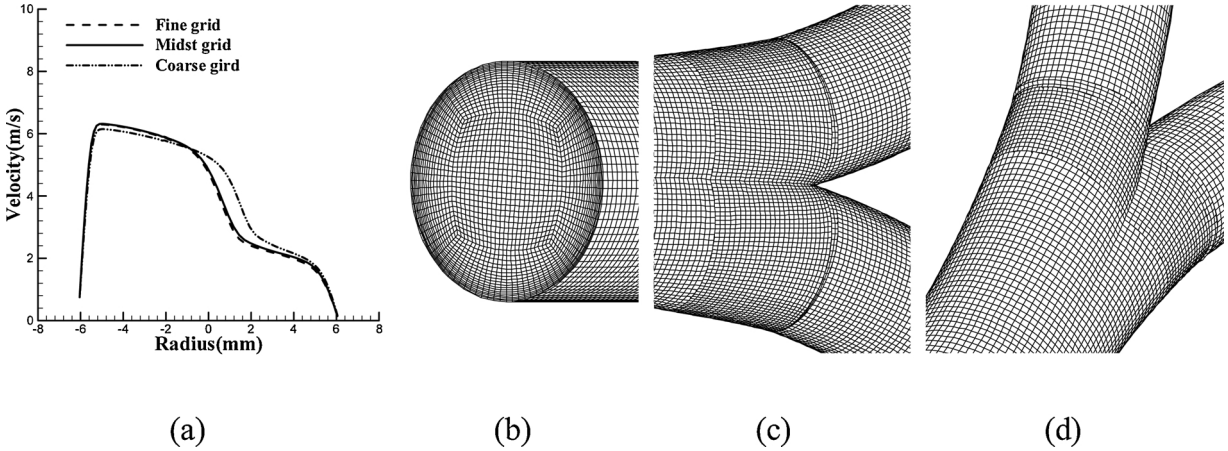

Fig. 5. Grid independence test and midst block-structured grid: **(a)** verification of grid independence at flow rate of 60 L/min; **(b)** local mesh in the G_0; **(c)** local mesh in first bifurcation region (G_0 to G_1); **(d)** local mesh in second bifurcation region (G_1 to G_2).

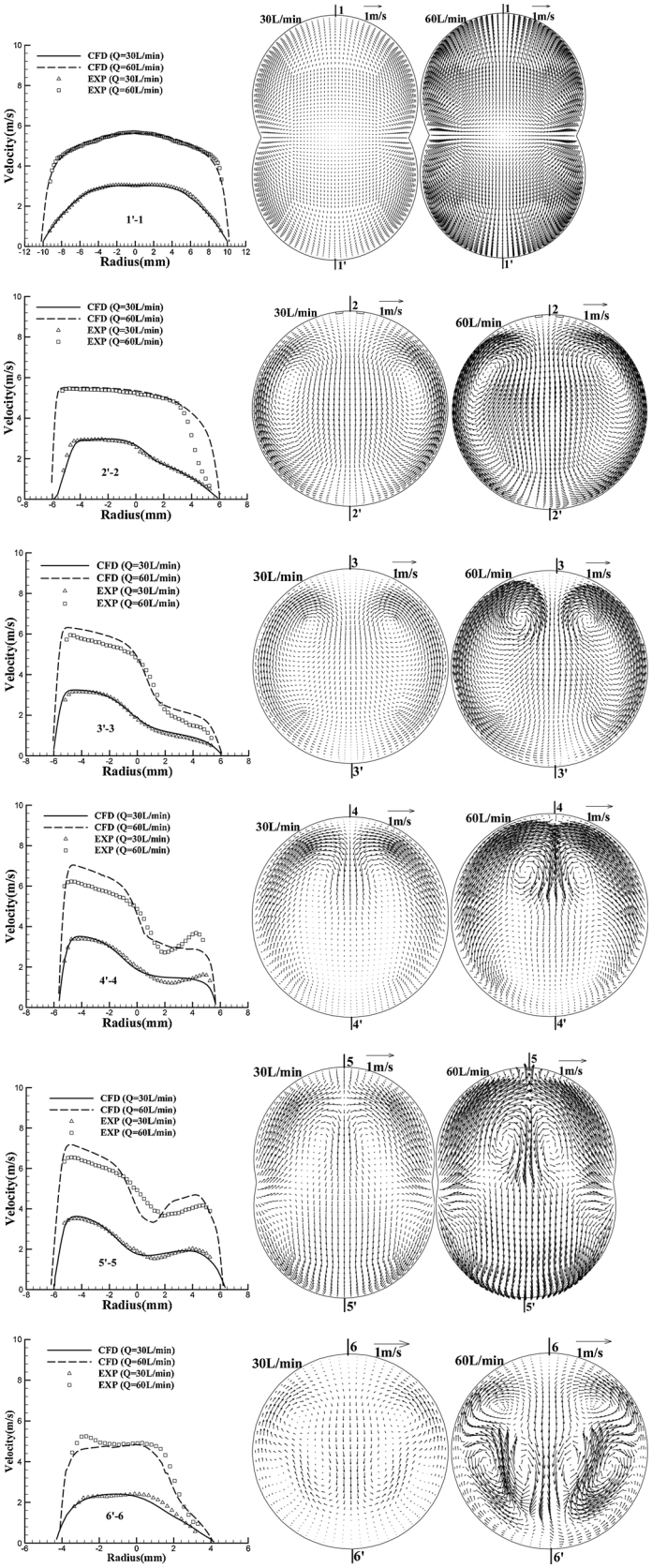

Fig. 7. The inspiration mainstream velocity profiles and secondary flows at seven cross sections, from 1′-1 to 7′-7.

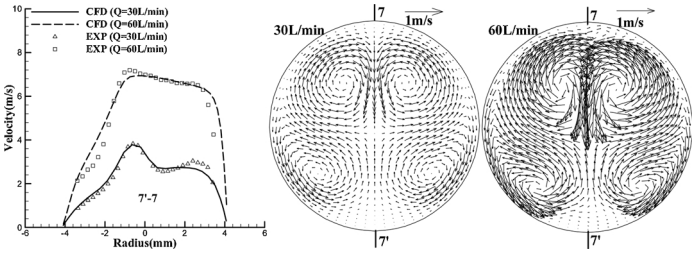

Fig. 7. (*continued*)

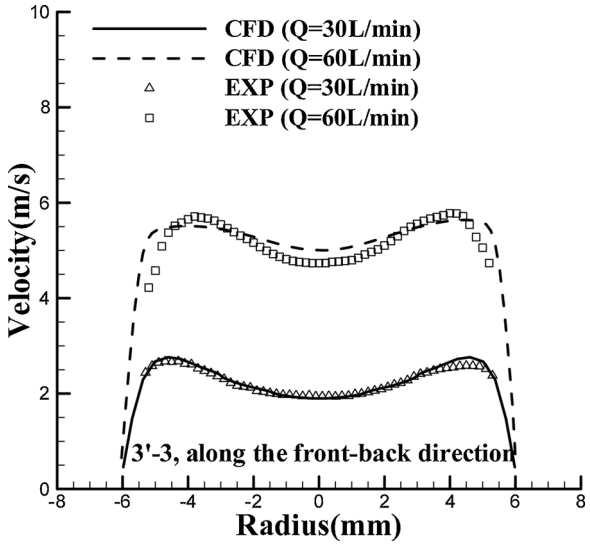

Fig. 8. The inspiration mainstream velocity profiles along the *z* direction at cross section 3'-3.

extracted from the measurements at cross section 0′-0 (Fig. 6). Fig. 7 presents the comparison of the mainstream velocity profile between the numerical and experimental results, and the calculated secondary flows at cross sections 1'-1 to 7′-7. At cross section 1'-1, within the transition zone of G_0-G_1, the inspiration flows are directed from the central region with higher momentum to the carinal side (side1′ and 1) with lower momentum. The similar flow patterns were confirmed in Zhao and Lieber, (1994a), Farag et al. (2000) and Jalal et al. (2016).

At the G_1 bronchia, four cross sections (from 2′-2 to 5′-5) are measured and compared against the numerical simulation. At cross section 2'-2, an obvious skewed distribution for the mainstream velocity profiles and Dean vortex for the secondary flows appear as a result of dual action of the upstream bifurcation and the wall curvature (Dean and Hurst, 1959). Suffered from the upstream bifurcation, new boundary layers are generated at the inner wall (side 2′, 3′, 4′, 5′) of G_1 (Kleinstreuer and Zhang, 2010). Even more skewed mainstream velocity profiles are observed at cross section 3'-3, due to further development of the secondary flow. The four-vortex secondary flows may be induced from the combined action of the wall curvature and the downstream bifurcation at cross section 4'-4. As a result, the mainstream velocity profiles turn into a double-peaked one (Farag et al., 2000; Luo and Liu, 2008; Kerekes et al., 2016). At cross section 5'-5, the double-peaked patterns are also observed both from the experimental and numerical results. The well-known jet-wake flow pattern, i.e., the jet flow near the inner and outer wall while the wake flow in the central region, will result in additional jet-wake mixing loss and thus increase the total pressure loss. The similar mainstream profiles at cross section 2'-2 and 3′-3 were also observed in Adler and Brücker (2007) with a similar geometry model and Reynolds number, however, the profiles at cross section 4'-4 and 5′-5 were not measured in their work.

At the G_2 bronchia, owing to the triple actions of the upstream bifurcation, the upstream jet-wake flow and the local wall curvature, both the mainstream velocity profiles and the secondary flows in G_2 are more complex than those in G_1. The jet fluid with relative lower momentum at the outer side (side 5) flows into the lateral branch (cross section 6'-6) while the jet fluid with relative higher momentum at the inner side (side 5′) flows into the medial one (cross section 7′-7). The secondary flows behave as two pair of Dean vortexes, i.e., four-vortex at cross section 7′-7, however, three pair vortexes, i.e., six-vortex at cross section 6'-6. The results show that the flow patterns in terms of both the mainstream and secondary flow will influence the flows in the even downstream generations.

The M-shaped profiles (*z* direction) are observed as a result of the Dean-type secondary flow in Fig. 8. The Dean-type secondary flows move the fluids with lower momentum at the outer wall side to the central region where the wake fluids are accumulated (Luo and Liu, 2008; Leong et al., 2009; Kerekes et al., 2016).

In summary, the agreement between the measurements and simulations of mainstream velocity profiles is generally good in the inspiration segment, especially at the 30 L/min flow rate. At the flow rate of 60 L/min, the local Reynolds number at the G0, G1 and G2 is 4410, 3308 and 2481, respectively, and the large variation in Reynolds numbers makes it very difficult for a single viscous model to match the complex laminar-transitional-turbulent flows. The mainstream velocity profiles are observed to have skewed and double-peaked patterns along the inner-outer direction, and M-shaped along the *z* direction. The combination of bifurcation, merge and curvature makes the Dean-type vortex structure even more complex. The basic Dean-type two-vortex is generated mainly due to the curvature. The four-vortex is generated mainly due to the bifurcation of the upstream two-vortex in inspiration stage. The six-vortex is generated by combination of asymmetric bifurcation and local curvature in inspiration stage. Due to the relative short length of each generation, the above vortex pattern will undergo the developing rather than the developed status. The inspiration flows in multi-generation human TB model are influenced by the combination of upstream and downstream bifurcation, local wall curvature and limited generation length.

5.2. Expiration

Instead of the bifurcating flows during the inspiration stage, the most remarkable flow feature during the expiation stage is the merging flows from the daughter branches into the mother branch. The results of the mainstream velocity profiles and secondary flow patterns at seven cross sections (from 7′-7 to1′-1) are shown in Fig. 9.

At the G_2, due to the imbalance mass-flux, both of the mainstream and secondary flow velocities at cross section 7′-7 are significantly higher than those at cross section 6'-6. The secondary flows are directed to the outer wall (7′ and 6). As a result, the mainstream velocity profiles are skewed towards the outer wall side.

At the G_1, the lower mass-flux fluids from the lateral branch (cross section 6'-6) merge with the higher ones from the medial branch (cross section 7′-7). At cross section 5'-5, double-peaked mainstream velocity profiles are observed. Four-vortex secondary flow patterns are observed, directing the lower momentum fluids towards the wake region.

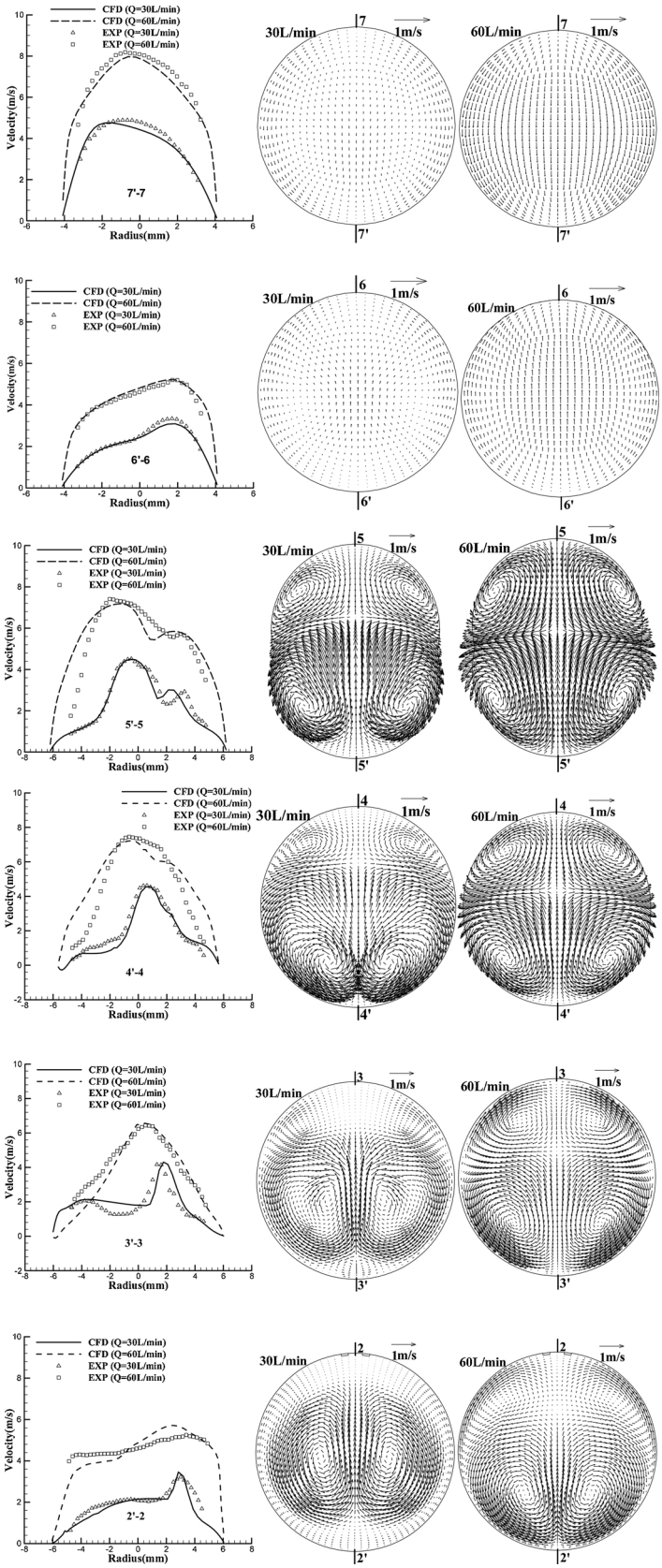

Fig. 9. The expiration mainstream velocity profiles and secondary flows at seven cross sections, from 7′-7 to 1′-1.

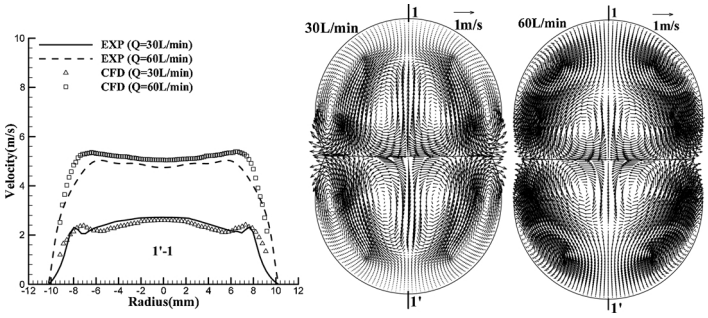

Fig. 9. (*continued*)

At cross section 4'-4, the wake flow almost disappears due to the jet-wake mixing effect and the mainstream velocity profiles behaves as skewed ones. At cross section 3'-3 and 2′-2, the higher momentum fluids move from the center region towards the outer side due to the secondary flows.

At the G_0, two streams of fluids with the same mass-flux from the two G_1 branches merge together. At cross section 1'-1, the mainstream velocity profiles are symmetric along the 1′-1 direction. Eight-vortex secondary flows are observed, which are inherited from four-vortex secondary flows (cross section 2'-2) in the two upstream branches. The numerical simulated results also indicate that, after the cross section 2'-2, the two pairs of vortexes near the wall will be mixed out quickly and the eight-vortex secondary patterns will change into the four-vortex ones with the flow developed.

Generally speaking the expiration flow, the numerical mainstream velocity profiles are in consistence with the LDV measurements at the two flow rates. Again, the agreement at 30 L/min flow rate is better than that at 60 L/min. The error between the measured and numerical results at 60 L/min is mainly due to the large variation in local Reynolds numbers. The mainstream velocity profiles with skewed, double-peaked, and the secondary flows with four-vortex and eight-vortex patterns are observed. The four-vortex is generated mainly due to the merge of upstream flow in expiration stage. The eight-vortex is generated by merge of the upstream four-vortex in expiration stage.

Overall, this work presents a detailed space-evolution of the mainstream and secondary flow patterns within an idealized three-generation TB airway model using the combination of LDV measurements and CFD simulations. Both of the inspiration and expiration flows are investigated with the same experimental rig and numerical model. A detailed time-evolution of unsteady respiratory flow at various breathing intensities and frequencies will add even more complication to both the experimental and numerical model, such as the alternate positive and negative flow rate condition at inlet and outlet boundaries. However, the present work contributes to an insight into the complex inspiration and expiration flow mechanism in terms of mainstream and secondary flow pattern, and can be regarded as a step-stone for a deep understanding of the respiratory physiology-related flow mechanisms.

6. Conclusion

The inspiration and expiration flows in a three-generation human lung TB model are experimentally measured with LDV technique and numerically simulated with CFD method. Two flow rates of 30 L/min and 60 L/min, corresponding to adult male breathing rates under light activity and moderate exercise conditions, are considered. The detailed space-evolution of the mainstream and secondary flow patterns within the three-generation TB airway model at the two flow rates are presented.

The comparison of the inspiration and expiration mainstream velocity profiles between the LDV measurements and CFD simulations are generally good, and the CFD method can be used to provide the more detailed flow fields in human lung TB model. From the comparative results with six viscous models, the respiration flows in human lung TB airway are even closer to the laminar one at the light activity condition while the turbulent one at the moderate exercise condition.

The mainstream flow in human lung TB airway is non-uniform and behaves as skewed, double-peaked and M-shaped patterns, while the secondary flow in human lung TB airway is complex and characteristic of Dean-type two-vortex, four-vortex, six-vortex and eight-vortex patterns. The inspiration and expiration flow patterns are heavily influenced by the combination of geometrical bifurcating/merging, local wall curvature, limited generation length and multi-generation interaction. This work can be regarded as a step-stone for a deep understanding of human lung physiology and associated flow mechanisms.

Acknowledgements

This work is financially supported by the National Key Research and Development Project of China under Grand No. 2016YFB0200901, National Natural Science Foundation of China under Grand No. 51776154, and Shaanxi Key Research and Development Project under Grant No. 2018KWZ-01.

References

Adams, C.F., Geoghegan, P.H., Spence, C.J., Jermy, M.C., 2018. Modelling nasal high flow therapy effects on upper airway resistance and resistive work of breathing. Respir. Physiol. Neurobiol. 254, 23–29.
Adler, K., Brücker, C., 2007. Dynamic flow in a realistic model of the upper human lung airways. Exp. Fluids 43, 411–423.
Banko, A.J., Coletti, F., Schiavazzi, D., Elkins, C.J., Eaton, J.K., 2015. Three-dimensional inspiratory flow in the upper and central human airways. Exp. Fluids 56, 1–12.
Corcoran, T.E., Chigier, N., 2002. Inertial deposition effects: a study of aerosol mechanics in the trachea using laser Doppler velocimetry and fluorescent dye. J. Biomech. Eng. 124, 629–637.
Dean, W.R., Hurst, J.M., 1959. Note on the motion of fluid in a curved pipe. Mathematika 6, 77–85.
Durst, F., Melling, A., Whitelaw, J.H., 1981. Principles and Practice of Laser Doppler Anemometry, 2nd ed. Academic Press, London.
Farag, A., Hammersley, J., Olson, D., Ng, T., 2000. Mechanics of the flow in the small and midst human airways. J. Fluids Eng. 122, 576–584.
Große, S., Schröder, W., Klaas, M., Klöckner, A., Roggenkamp, J., 2007. Time resolved analysis of steady and oscillating flow in the upper human airways. Exp. Fluids 42, 955–970.
Jalal, S., Nemes, A., Van de Moortele, T., Schmitter, S., Coletti, F., 2016. Three-dimensional inspiration flow in a double bifurcation airway model. Exp. Fluids 57, 1–15.
Jayaraju, S.T., Brouns, M., Verbanck, S., Lacor, C., 2007. Fluid flow and particle deposition analysis in a realistic extrathoracic airway model using unstructured grids. J. Aerosol Sci. 38, 494–508.
Kerekes, A., Nagy, A., Veres, M., Rigó, I., Farkas, Á., Czitrovszky, A., 2016. In vitro and in silico (IVIS) flow characterization in an idealized human airway geometry using laser Doppler anemometry and computational fluid dynamics techniques. Measurement 90, 144–150.
Kleinstreuer, C., Zhang, Z., Li, Z., 2008. Modeling airflow and particle transport/deposition in pulmonary airways. Respir. Physiol. Neurobiol. 163, 128–138.
Kleinstreuer, C., Zhang, Z., 2009. An adjustable triple-bifurcation unit model for air-particle flow simulations in human tracheobronchial airways. J. Biomech. Eng. 131 021007–021007-10.
Kleinstreuer, C., Zhang, Z., 2010. Airflow and particle transport in the human respiratory system. Annu. Rev. Fluid Mech. 42, 301–334.
Leong, F.Y., Smith, K.A., Wang, C.H., 2009. Secondary flow behavior in a double bifurcation. Phys. Fluids 21 043601-1–043601-11.
Li, C., Jiang, J., Dong, H., Zhao, K., 2017. Computational modeling and validation of

human nasal airflow under various breathing conditions. J. Biomech. 64, 59–68.
Liu, Y., So, R.M.C., Zhang, C.H., 2002. Modeling the bifurcating flow in a human lung airway. J. Biomech. 35, 465–473.
Liu, Y., So, R.M.C., Zhang, C.H., 2003. Modeling the bifurcating flow in an asymmetric human lung airway. J. Biomech. 36, 951–959.
Lizal, F., Jedelsky, J., Morgan, K., Bauer, K., Llop, J., Cossio, U., Kassinos, S., Verbanck, S., Ruiz-Cabello, J., Santos, A., Koch, E., Schnabel, C., 2018. Experimental methods for flow and aerosol measurements in human airways and their replicas. Eur. J. Pharm. Sci. 113, 95–131.
Luo, H.Y., Liu, Y., 2008. Modeling the bifurcating flow in a CT-scanned human lung airway. J. Biomech. 41, 2681–2688.
Menter, F.R., 1994. Two-equation eddy-viscosity turbulence models for engineering applications. AIAA J. 32, 1598–1605.
Pedley, T.J., 1977. Pulmonary fluid dynamics. Annu. Rev. Fluid Mech. 9, 229–274.
Schiavazzi, D.E., Nemes, A., Schmitter, S., Coletti, F., 2017. The effect of velocity filtering in pressure estimation. Exp. Fluids 58, 1–21.
Weibel, E.R., 1963. Morphometry of the Human Lung. Academic Press, New York.
Zhang, Z., 2010. LDA Application Methods: Laser Doppler Anemometry for Fluid Dynamics. Springer, Berlin.
Zhang, Z., Kleinstreuer, C., 2003. Low-Reynolds-number turbulent flows in locally constricted conduits: a comparison study. AIAA J. 41, 831–840.
Zhao, Y., Lieber, B.B., 1994a. Steady inspiration flow in a model symmetric bifurcation. J. Biomech. Eng. 116, 488–496.
Zhao, Y., Lieber, B.B., 1994b. Steady expiration flow in a model symmetric bifurcation. J. Biomech. Eng. 116, 318–323.